ACS OMEGA

Article

Cite This: ACS Omega 2019, 4, 21431−21438

http://pubs.acs.org/journal/acsodf

# Ultrasensitive Detection of Severe Fever with Thrombocytopenia Syndrome Virus Based on Immunofluorescent Carbon Dots/$SiO_2$ Nanosphere-Based Lateral Flow Assay

Lai-Di Xu,[†] Qing Zhang,[‡] Shou-Nian Ding,*[,†] Jing-Juan Xu,[§] and Hong-Yuan Chen[§]

[†]Jiangsu Province Hi-Tech Key Laboratory for Bio-medical Research, School of Chemistry and Chemical Engineering, Southeast University, Nanjing 211189, China

[‡]Chinese Academy of Inspection and Quarantine, Beijing 100176, China

[§]State Key Laboratory of Analytical Chemistry for Life Science and Collaborative Innovation Center of Chemistry for Life Sciences, School of Chemistry and Chemical Engineering, Nanjing University, Nanjing, 210023, China

Supporting Information

**ABSTRACT:** Sensitive detection of severe fever with thrombocytopenia syndrome virus (SFTSV) by a point-of-care assay is of great significance for promoting clinical diagnosis. In this work, ultrasensitive detection of SFTSV was achieved by using fluorescent carbon dots/$SiO_2$ nanospheres (CSNs) as reporters for a lateral flow assay. The prepared CSNs were resistant to extreme environments and had strong stability. The uniform CSNs with the size of about 200 nm were obtained by differential centrifugation. Their absolute quantum yields in the aqueous and solid phases are 56.3 and 36.6%, respectively. The excellent fluorescent properties of CSNs make the test strips more sensitive and have a longer assay lifetime. Thus, the visual detection limit of the lateral flow test strip based on immunofluorescent CSN (iCSN) was as low as 10 pg/mL SFTSV nucleoprotein. The sensitivity of this assay is 2 orders of magnitude higher than that of the colloidal gold-based lateral flow test strip. Besides, the assay owns good reproducibility and high specificity. Then, iCSN-based lateral flow test strips were evaluated in real samples of human serum of patients with satisfactory results. Furthermore, this assay has a general prospect for other fluorescent immunochromatography applications.

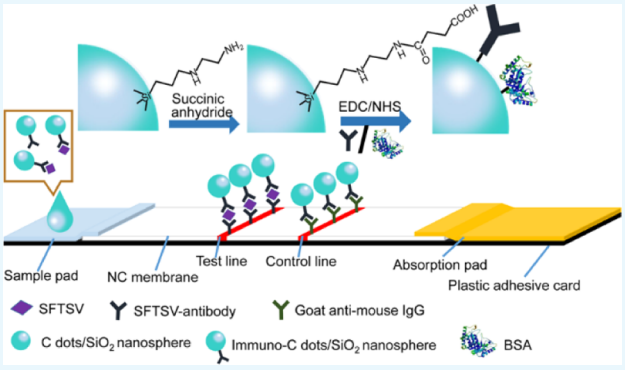


## INTRODUCTION

Severe fever with thrombocytopenia syndrome (SFTS) is an emerging infectious disease with fever, thrombocytopenia, and leukopenia as the main clinical symptoms.[1] Since 2010, it has caused human infection and death in central and eastern China. A novel Bunia virus, also known as SFTS virus (SFTSV), has been found to be the cause of the disease. SFTSV is a single negative strand RNA virus whose genome contains three RNA circular fragments of large (L), medium (M), and small (S). The S fragment is an ambisense, encoding a nucleoprotein (NP) and a nonstructural protein. NP can encapsulate three RNA genomic fragments of SFTSV and play an important role in viral transcription and replication.[2] In recent years, different SFTSV detection methods have been reported,[3−5] for example, the ELISA detection of SFTSV has been reported, which could detect an antigen concentration of 1 ng/mL. However, the lengthy and cumbersome operations and expensive instruments limit their practical application. In our previous work, colloidal gold-based lateral flow assay was used for simple, convenient, and rapid detection of SFTSV with a visual detection limit of 1 ng/mL SFTSV NP.[6]

As the most famous point-of-care (POC) assay strategy, lateral flow assay has been successfully utilized for detecting small molecules,[7,8] nucleic acids,[9] proteins,[10,11] and so on. The main advantages of the lateral flow test strip are speed, low cost, simplicity, convenience, and no need for trained personnel and expensive equipment.[11] The lateral flow test strips labeled with gold nanoparticles have been widely used and commercialized. This is due to their excellent stability, incomparable biocompatibility, simpler synthesis, visual results, and more. However, the inherent low signal-to-noise ratio of gold nanoparticles limits their lower detection limit.[12]

Up to now, researchers have further developed lateral flow test strips using magnetic materials,[13,14] carbon materials,[15−17] fluorescent quantum dots (QDs),[18,19] upconversion phosphors,[20,21] and organic fluorescent dyes[22] as signal materials to improve sensitivity. Among them, the integration of fluorescent QDs into nanospheres will further improve the sensitivity,

Received: September 23, 2019
Accepted: November 14, 2019
Published: December 2, 2019




DOI: 10.1021/acsomega.9b03130
ACS Omega 2019, 4, 21431−21438

because the fluorescence intensity of a fluorescent nanosphere is much higher than that of a single QD. Furthermore, fluorescent nanospheres possess good biocompatibility, high stability in a complex matrix, and convenient manipulation compared with traditional semiconductor QDs.[23] Over the past decade, many researchers have worked on the construction and application of semiconductor QDs-based fluorescence nanospheres and have achieved a series of achievements.[24−31] Different construction methods always have various limitations.[23,32] For instance, after embedding high-quality oil QDs into nanospheres, QDs may leak out of the sphere pores in nonpolar suspended media. The incorporating of QDs during the nanosphere formation process usually requires careful control of the reaction conditions, and QDs may aggregate during the polymerization, which may affect their fluorescence properties. The process of assembling QDs onto the surface of the nanospheres is cumbersome and time-consuming, and it usually requires an additional shell to cover the resulting fluorescent spheres for protection and conjugation.

Most studies on carbon materials as signal reporters for test strips mainly include carbon colloids and carbon nanotubes, which can help to visually observe the test results.[15,16,33−35] They are more sensitive, stable, and environmentally friendly than gold particles. Fluorescent carbon dots (CDs) are a member of QDs and are a new class of zero-dimensional nanomaterials in the carbon family. Compared with conventional semiconductor QDs, fluorescent CDs are superior in terms of chemical inertness, photostability, low cytotoxicity, and biocompatibility.[36−38] Therefore, CDs can be widely used in biological imaging,[38−42] drug release,[43] as a sensor,[44] photocatalyst,[45] and so on. Identically, the sensitivity of fluorescent carbon spheres as the test strip signal should be higher than that of fluorescent CDs as the test strip signal. To our best knowledge, there is no report of the use of fluorescent CDs-based nanospheres as tags on the lateral flow test strip.

In this paper, we reported a rapid and sensitive method for the detection of SFTSV based on immunofluorescent CDs/$SiO_2$ nanospheres (iCSNs) coupled with lateral flow test strips. The pathogen SFTSV of SFTS syndrome was used as a model virus. The initial symptoms of the SFTS syndrome are difficult to distinguish from viral infections such as influenza. Amino-rich fluorescent CDs/$SiO_2$ nanospheres (CSNs) were synthesized by simple co-hydrolysis of silanized CDs with tetraethyl orthosilicate (TEOS). It has excellent fluorescence performance and stability, and greatly improves the sensitivity of the test strip. As expected, the detection limit of the assay was 10 pg/mL, which is 2 orders of magnitude lower than that of the colloidal gold immunochromatography assay, indicating that the iCSN-based test strip is promising in practice.

## RESULTS AND DISCUSSION

**Characterization of the CSNs.** CSNs were prepared by co-hydrolysis of CDs and TEOS. The disadvantage of this method is that the uniformity of the material is not good.[46] In order to overcome the non-uniformity of CSNs, CSNs with uniform morphology were obtained by differential centrifugation. Figure 1 illustrates transmission electron microscopy (TEM) images of CSNs obtained by differential centrifugation. It can be seen that the particles exhibit good dispersibility, and as the separation speed increases from low to high, the size of the particles obtained at each rotational speed is remarkably reduced. The precipitate at 1500 rpm is mostly agglomerated particles as well as larger particles. When the rotating speed increased to 2000 rpm, there were still some agglomeration particles in the precipitate. When the rotating speed is further increased to 2500 rpm, the precipitated particle size is uniform and does not aggregate, and the average particle size is 200 nm. In addition, there are many smaller particles in the supernatant at 2500 rpm. The precipitate obtained at 2500 rpm was used as the next research object. The image of high-resolution TEM (HRTEM) in Figure 1E shows that CSNs own a mesoporous structure. CDs cannot be observed directly by HRTEM. This can be attributed to the molecular-level chemical dispersion of CD molecules in the silica matrix.[47] The incorporation of CDs into the formation of $SiO_2$ nanospheres does not affect the fluorescence properties of CDs, and the strong fluorescence emitted by CSNs can be clearly visualized under a confocal fluorescent microscope (Figure 1F). The absolute quantum yields of CSNs in the aqueous phase and in the solid state are as high as 56.3 and 36.6%, respectively. Compared with the quantum yield of CDs of 47%,[39] the quantum yield of CSNs in the aqueous phase is higher. This indicates that the obtained CSNs have good stability and can be applied in harsh environments such as strong acids.

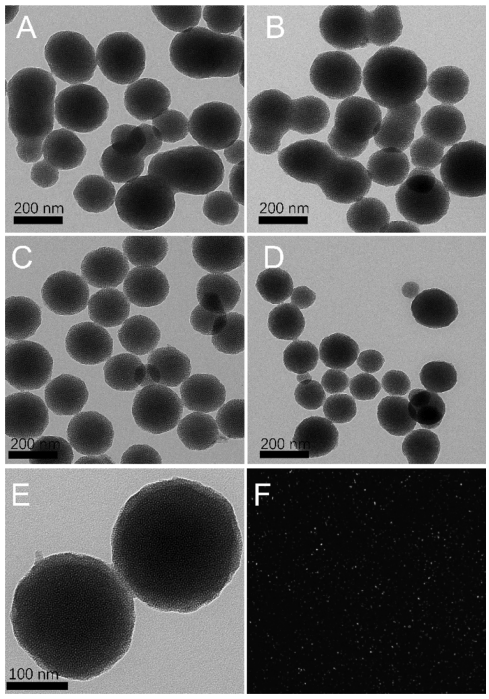


**Figure 1.** TEM images of the precipitates obtained by separating the CSNs at 1500 (A), 2000 (B), and 2500 rpm (C), and the supernatant at 2500 rpm (D). HRTEM (E) and confocal fluorescent image (F) of the precipitate obtained at 2500 rpm.

As demonstrated in Figure 2, the intense blue light of the CD aqueous solution, the CSN aqueous solution, and the CSN powder can be observed under a 360 nm ultraviolet (UV) lamp. When excited in the range of 360−400 nm, the CD aqueous solution, the CSN aqueous solution, and the CSN powder exhibit strong blue photoluminescence (PL) centered at approximately 460 nm. When the excitation wavenumber is further increased, the emission of the CDs shifts from 465 to 524 nm and accompanied by a remarkable decrease in PL intensity, whereas the PL center of the CSN aqueous solution and the CSN powder does not move significantly; there is only a significant decrease in PL intensity. The PL centers of the


DOI: 10.1021/acsomega.9b03130
ACS Omega 2019, 4, 21431−21438

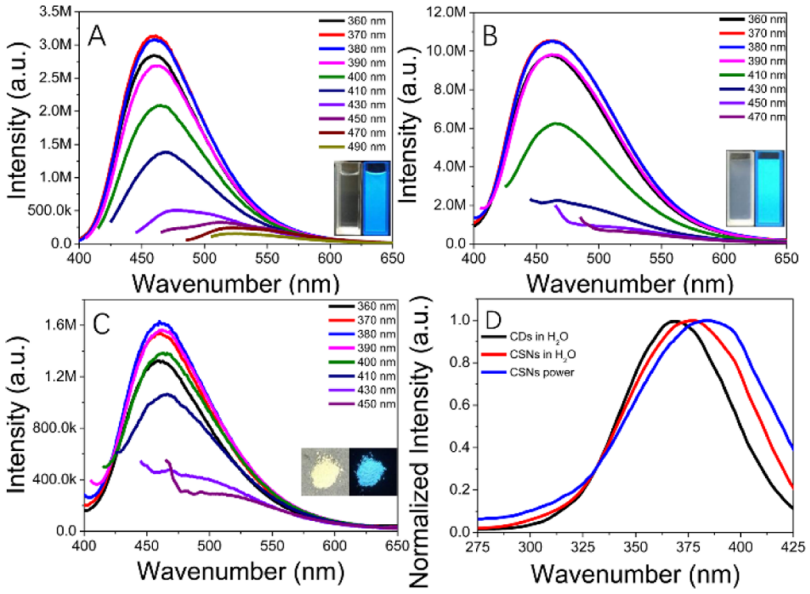


**Figure 2.** Emission spectra of (A) CDs in $H_2O$, (B) CSNs in $H_2O$, and (C) CSNs power at different excitation wavenumbers and the corresponding photos under sunlight (left insert) and a 360 nm UV light (right insert). Corresponding excitation spectra (D).

CD aqueous solution, the CSN aqueous solution, and the CSN powder excited at 360 nm are 459, 462, and 463 nm, respectively. The optimum excitation wavelengths of the CD aqueous solution, the CSN aqueous solution, and the CSN powder are 369, 377, and 384 nm, respectively (Figure 2D). The red shift of the CSN aqueous solution relative to the CD aqueous solution is due to the increase in the rigidity of the CDs caused by CDs embedded in the rigid support of silica,[47] enhanced molecular structure rigidity, increased coplanarity, and enhanced emission.[48,49] The aggregation of CDs caused by solvent volatilization leads to further red shift of the CSN powder.[50] Energy resonance transfer or direct $\pi-\pi$ interaction occurs because of the decrease of distance between adjacent CDs, which leads to the decrease of fluorescence efficiency.[51] In addition, *N*-$\beta$-(aminoethyl)-$\gamma$-aminopropyltrimethoxysilane (AEAPTMS), as a long-chain ligand, has a strong steric hindrance effect, and the CDs are embedded in the silica matrix, which makes the CDs support each other in the solid state and weakening the agglomeration effect, so the solid CSNs have fluorescence properties.

**Fabrication of an iCSN-Based Lateral Flow Test Strip.** To explore the feasibility of CSNs in sensitive fluorescence detection, CSNs were applied as optical labels on the lateral flow test strip. The first was to conjugate CSNs with the antibody. The composition of the CD is calculated by theory (Supporting Information, S4), which contains a large number of AEAPTMS. In the synthesis of CSNs, AEAPTMS participated in the reaction, so the CSNs are rich in amino groups. Although the glutaraldehyde method can directly bind the amino-rich CSNs to the antibody to form a complex, in the coupling process, agglomeration easily occurs among antibodies, antibodies and CSNs, and CSNs. Therefore, the particle size of the CSNs is greatly increased to the micron level, which is not suitable for immunochromatography (Figure S3A). This work was carried out by the succinic anhydride method, that is, the amino groups of CSNs were first reacted with succinic anhydride to form succinic acid half esters, which were then catalyzed by carbodiimide to form amide bonds with antibody (Figure 3A). The zeta potential of CDs/$SiO_2$ spheres altered

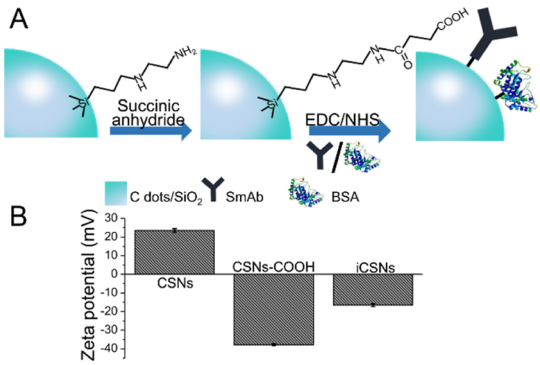


**Figure 3.** (A) Schematic illustration of the surface functionalization of the CSNs for lateral flow immunoassay. (B) Zeta potential of the CSNs at different stages of surface functionalization corresponding to panel (A).

successively from the 23.5 to −37.8 mV (Figure 3B), indicating that the surface of the CSNs is rich in amino groups and then successfully grafted with the carboxyl groups. The CSNs were then modified with SFTSV monoclonal antibody (SmAb) and further blocked with bovine serum albumin (BSA) to form iCSNs as reporters, resulting in a partially neutralized zeta potential (−16.6 mV).

As shown in Figure 4A, the pretreated sample pad, the nitrocellulose (NC) membrane, and the absorbent pad were adhered to the black plastic adhesive card to form a lateral flow test strip. The test (T) and control (C) lines of the NC membrane were coated with SmAb and goat antimouse IgG antibody, respectively. Figure 4B shows a schematic diagram of the SFTSV detection. The immunocomplex was formed by mixing the iCSNs with the sample and the mixture was then loaded into the sample pad to begin the test. The mixture was absorbed and migrated along the strip by capillary force. Through the interaction of specific antigen and antibody, the immunocomplex was captured by the T line on NC membrane to form the iCSN/SFTSV NP/SmAb sandwich structure. As the liquid continued to migrate, the free iCSNs moved further and were trapped by the goat antimouse IgG antibody on the



DOI: 10.1021/acsomega.9b03130
*ACS Omega* 2019, 4, 21431−21438

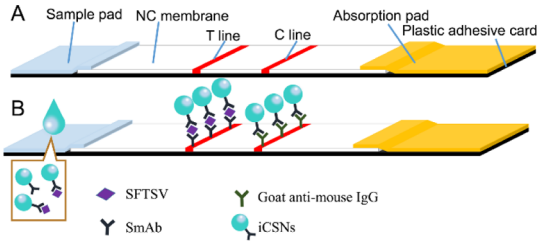


**Figure 4.** (A) Schematic illustration the configurations of iCSN-based test strip. (B) Schematic illustration of the detection of SFTSV using the iCSN-based test strip.

C line to form the iCSN/IgG structure. Because of the strong PL performance of CSNs, signals could be observed under a UV lamp. If there is no SFTSV NP in the sample, iCSNs will flow through the T line instead of accumulating on the T line, only interacting with the goat antimouse IgG antibody on the C line. The determination of the results is illustrated in Figure 5A. The sample is considered positive when two fluorescence

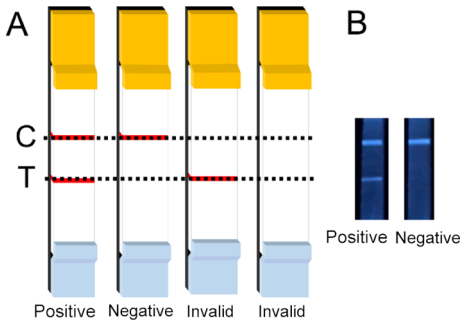


**Figure 5.** (A) Interpretation of results of the iCSN-based test strip. (B) Photos of iCSN-based test strips under UV lamp in the presence (left) and absence (right) of SFTSV.

lines appeared on the T and C lines, and negative when only the C line is seen. An invalid test is the one with only a T line or no lines. Figure 5B shows a picture of positive and negative results. For a positive result, the T and C lines show blue light under a UV lamp. For a negative result, only the C line shows blue light under a UV lamp.

**Performance of the iCSN-Based Lateral Flow Test Strip.** Sample pads were preimmersed in a buffer containing NaCl to eliminate false-positives before testing (Figure S3B). The possible reason is that secondary amines on CSNs and negatively charged amino acids on proteins may adsorb nonspecifically by electrostatic interactions. The salt dissociates into a positively charged and a negatively charged ionic state in water, which shields the protein from solid carriers and reduces nonspecific adsorption.[52,53] Under optimized detection condition, the sensitivity of the iCSN-based lateral flow test strip assay was investigated. First, a series of 60 $\mu$L SFTSV NP standards (1 $\mu$g/mL, 100 ng/mL, 10 ng/mL; 1 ng/mL, 100 pg/mL, 10 pg/mL, 0 pg/mL) were mixed with 10 $\mu$L of iCSN dispersion in a 0.5 mL centrifuge tube, respectively. The mixtures were then loaded separately onto the sample pads of the lateral flow test strips. As shown in Figure 6A, the blue C lines demonstrate the validity of the test results. The brightness of the T line decreases as the concentration of SFTSV NPs decreases. From 1 $\mu$g/mL to 1 ng/mL, the T lines emits very bright blue light, indicating positive results immediately. The colors of T lines are hard to be distinguished under low

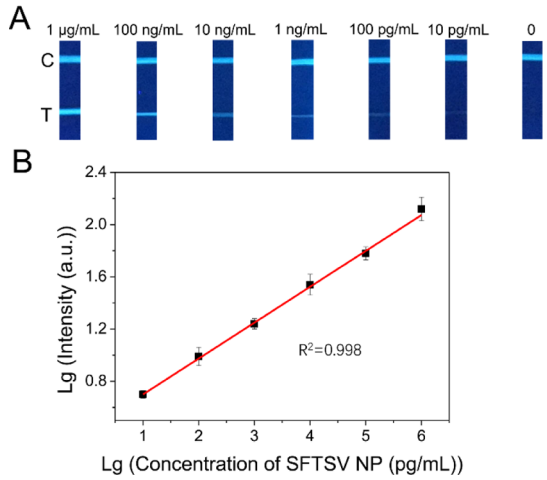


**Figure 6.** Sensitivity of the lateral flow assay for quantification of SFTSV NP. (A) Fluorescence pictures of the test strips for 1 $\mu$g/mL, 100 ng/mL, 10 ng/mL, 1 ng/mL, 100 pg/mL, 10 pg/mL, and 0 pg/mL standard SFTSV NP in buffer. (B) iCSN-based lateral flow test strip's linear response for SFTSV NP detection; concentration range of 10 pg/mL to 1 $\mu$g/mL in buffer.

concentrations. In addition, only the C line is observed in the absence of SFTSV NP. Here, the visual detection limit for detecting SFTSV NPs is 10 pg/mL. The extremely low detection limit of the lateral flow test strip based on CSNs can be attributed to the excellent fluorescence characteristics of CSNs. This test can be quantified by estimating the brightness of the T line. As shown in Figure 6B, a linear relationship is obtained in a wide range of 10 pg/mL to 1 $\mu$g/mL with a linear correlation coefficient ($R^2$) of 0.998. Compared to the previous SFTSV detection methods (Table S1), our method utilizes the novel cost-effective materials, saves time, and has a decent performance at the same time. This suggests that the iCSN-based lateral flow test strips have very promising prospects for high-sensitivity POC detection of viruses.

To confirm the selectivity of the current immunoassay, blank phosphate buffer solution (PBS) and five different antigens with a concentration of 1 $\mu$g/mL were examined on the strip individually. The five antigens were HCG, AFP, CEA, CA125, and SFTSV NP. As shown in Figure 7, only the T line of the SFTSV NP shows obvious color. Accordingly, the fluorescence intensity for the SFTSV NP sample is conspicuously higher than that for those nonspecific protein samples. These results mean that the iCSN-based lateral flow test strip can specifically detect SFTSV.

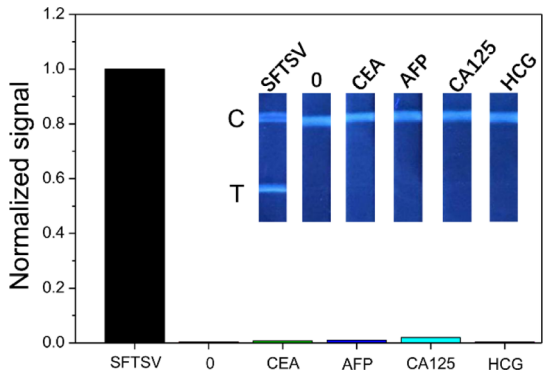


**Figure 7.** Specificity research results to different interfering proteins.



DOI: 10.1021/acsomega.9b03130
ACS Omega 2019, 4, 21431−21438

To evaluate the precision and reproducibility of the iCSN-based test strip, the intra-assay and interassay were performed using 1 μg/mL, 10 ng/mL, and 100 pg/mL SFTSV NP standard samples. The intra-assay CV and inter-assay CV are 4.8 and 7.1% (Table 1), respectively, demonstrating that the method has high reproducibility and good precision. The strong stability of CSNs keeps its fluorescence intensity constant as the storage time increases, and even after 6 months of storage, iCSN retains its biological activity when used in test strips (Figure 8).

**Table 1. Reproducibility Analysis of the iCSN-Based Test Strip**

| SFTSV NP concentration | intra-assay | | | interassay | | |
|---|---|---|---|---|---|---|
| | mean[a] | SD[b] | CV[c] (%) | mean[a] | SD[b] | CV[c] (%) |
| 1 μg/mL | 131.8 | 6.0 | 4.5 | 145 | 9.2 | 6.3 |
| 10 ng/mL | 34.6 | 1.7 | 4.9 | 33 | 2.3 | 7.0 |
| 100 pg/mL | 9.8 | 0.5 | 5.1 | 11 | 0.9 | 8.1 |
| | intra-assay variability 4.8% | | | inter-assay variability 7.1% | | |

[a]Values represent the average of detected fluorescence intensities of parallel samples ($n$ = 3). [b]Values represent the standard deviation of parallel results ($n$ = 3). [c]CV = SD/mean.

Taken together, the above results show that the detection method possessed high sensitivity, high stability, good selectivity, and good reproducibility.

**Detection of SFTSV in Human Serums.** To evaluate the application of the iCSN-based lateral flow test strip in clinical diagnosis, the immunoassay was extended to the clinical diagnosis of SFTSV in serum as in our previous work.[6] The results of the real-samples analysis (Figure 9) are consistent with the results of the polymerase chain reaction and the colloidal gold immunochromatographic test (Table 2), indicating that the iCSN-based lateral flow assay of human samples is reliable. Therefore, these results indicated that the iCSN-based lateral flow assay platform may bring a tremendous infusion of promise to the rapid detection of SFTSV in the early stages of the SFTS syndrome.

**Ethical Statement.** Human serum was collected from 10 mL of peripheral blood from volunteers in the First People's Hospital of Jiangsu Province, and only applied for scientific research. All protocols involving human subjects were reviewed and approved by the Ethical Committee of the Southeast University in accordance with the Declaration of Helsinki (Association, 2000). Informed consent was obtained from all human subjects enrolled in this study.

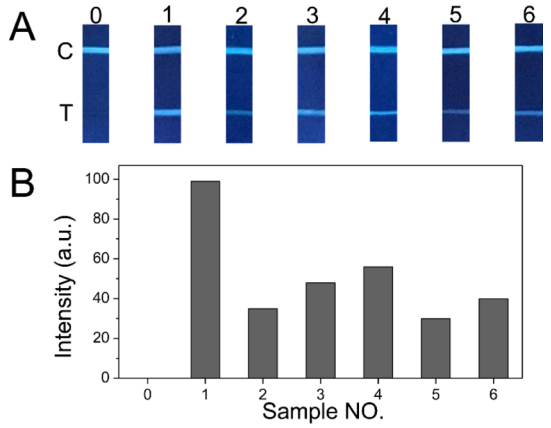


**Figure 9.** Fluorescence images (A) and histograms of the intensity of the corresponding T-lines (B) of real samples analysis by the iCSN-based lateral flow test strip.

**Table 2. Analysis of SFTSV in Human Serum by the iCSN-Based Lateral Flow Test Strip[a]**

| sample | control | 1 | 2 | 3 | 4 | 5 | 6 | |
|---|---|---|---|---|---|---|---|---|
| test results | − | + | + | + | + | + | + | PCR method |
| | − | + | + | + | + | + | + | gold nanoparticles-based test strip[6] |
| | − | + | + | + | + | + | + | our method |

[a]Note: (−) negative result, (+) positive result.

## CONCLUSIONS

In summary, fluorescent CSNs were prepared by co-hydrolysis of silanized CDs and TEOS using cetyltrimethylammonium bromide (CTAB) as a template, and uniform size CSNs were obtained by differential centrifugation. Compared with other fluorescent nanospheres, CSNs synchronously fulfill several criteria: homogeneously distributed CDs within $SiO_2$ templates, uniform dimensions for good reproducibility, convenient surface derivations, relatively simple preparation process, low cost, and environmental friendliness. In addition, it undergoes a strong acid and alkali environment during the synthesis process, but still has a strong quantum yield. The high absolute quantum yields of the CSNs in the aqueous phase and the solid phase make the test strip more sensitive

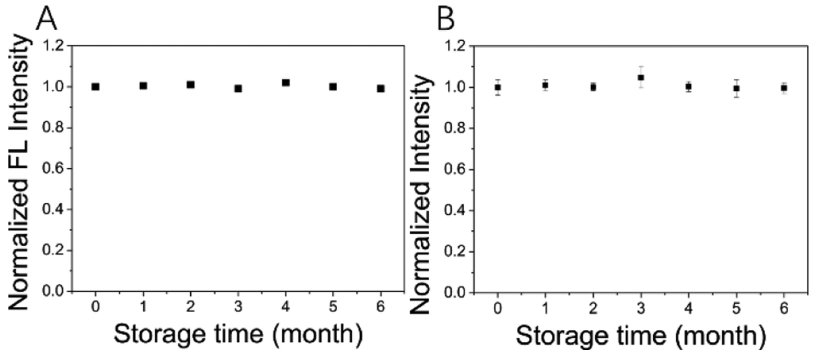


**Figure 8.** (A) Fluorescence intensity of the CSNs at different storage times. (B) Stability test of the iCSNs at different storage times.



DOI: 10.1021/acsomega.9b03130
ACS Omega 2019, 4, 21431−21438

and have a longer assay lifetime. The detection limit of the iCSN-based lateral flow test strip for SFTSV NPs was as low as 10 pg/mL. This is 2 orders of magnitude lower than the SFTSV NPs detected by the test strip of gold colloid as a signal. The assay exhibited a fast, sensitive, and highly selective response to the SFTSV and was applied to the detection of real samples. This assay opens up a new possibility for POC SFTSV detection in daily life. With the continuous expansion of future research, the detection principle can be extended to other virus, protein biomarkers, nucleic acids, and bacteria in clinical diagnosis and a variety of other biomedical applications, which have a wider clinical application prospect.

## EXPERIMENTAL SECTION

**Materials and Apparatus.** AEAPTMS, citric acid monohydrate, sodium hydroxide, CTAB, TEOS, succinic anhydride, hydrochloric acid (HCl), absolute ethanol, and *N*,*N*-dimethylformamide (DMF) were purchased from Sinopharm Chemical Reagent Co., Ltd. *N*-(3-Dimethylaminopropyl)-*N*′-ethylcarbodiimide hydrochloride (EDC) was purchased from Energy Chemical Co., Ltd. *N*-Hydroxysulfosuccinimide sodium salt (NHS) was purchased from Alfa Aesar Chemicals Co., Ltd. 2-(*N*-Morpholino)ethanesulfonic acid (MES) and 4-(2-hydroxyethyl)-1-piperazineethanesulfonic acid (HEPES) were purchased from Sigma-Aldrich. The $H_2O$ used in the experiment was double-distilled $H_2O$. BSA was obtained from Sangon Biotech Co., Ltd. SFTSV NP and SmAb were purchased from Jiangsu Center for Disease Control and Prevention. Goat antimouse IgG antibody, sample pads, NC membranes, absorbent pads, and black plastic adhesive cards were purchased from Shanghai JieYi Biotechnology Co. Ltd. (Shanghai, China). Serums of patients infected with SFTSV and normal human serums were supplied by Jiangsu Province Hospital. Data of serum detection using the PCR method were provided by Jiangsu Province Hospital. In addition, other apparatus are shown in the Supporting Information.

**Fabrication of CSNs.** At first, silanized CDs were synthesized according to the previous report with slight modifications.[39,46] The specific procedure was as follows: 15 mL of AEAPTMS was poured into a 50 mL three-necked flask and purged with nitrogen for 15 min. The solution was then heated to 240 °C, and 1 g of dehydrated citric acid (pretreatment of citric acid monohydrate in an 80 °C vacuum oven overnight) was quickly added with vigorous stirring. After 5 min, the heating was stopped and the solution was naturally cooled. The obtained CD solution was centrifuged at 10 000 rpm for 10 min to remove large particles at the bottom.

Then, CSNs were prepared by the co-hydrolysis method according to the previous report with modification.[39] In brief, CTAB (0.2 g) and NaOH (0.15 mL, 10 M) were added into 99 mL of $H_2O$ and stirred at 80 °C for 1 h. A mixture of TEOS (1.2 mL) and CD (0.35 mL) was quickly poured into the solution and allowed to stir at 80 °C for 3 h. The mixture was diluted with ethanol and collected by centrifugation. The precipitate was dispersed in a mixture of HCl (15 mL) and ethanol (120 mL) and stirred at 60 °C for 6 h to extract the residue organic template. The extraction was repeated once and the product was washed to neutral, and finally the aminoterminated CSNs were dispersed in ethanol.

Uniform-sized CSNs were obtained by differential centrifugation, that is, by gradually increasing the rotating speed from low to high. First, the CSNs with the largest size were separated from the solution at low speed, and then the liquid was poured into another centrifugal tube to increase the rotating speed and separate the CSNs in second order. With gradually increased rotating speed and repeating the above process, CSNs of size from large to small were obtained from the precipitation of each rotating speed. In order to improve the separation accuracy, the precipitation obtained at each rotating speed was dispersed and centrifuged several times under the same centrifugal conditions (the same speed and time), so that the small particles in the precipitation were gradually removed from the liquid through multiple dispersion, whereas the large particles were always retained in the precipitation. In the specific experimental process, the rotating speeds were 1000, 1500, 2000, 2500 rpm, respectively, the time was 15 min, and the solvent was ethanol. The bottom precipitate at 1000 rpm was discarded and the bottom precipitate at 1500, 2000 and 2500 rpm and the supernatant at 2500 rpm were separately studied.

**Fabrication of CSNs−Antibody Conjugates.** CSNs obtained at 2500 rpm were used as labels and conjugated to the SmAb. The aminoterminated CSNs were centrifuged and dispersed in DMF at a concentration of 1 mg/mL. Then, CSNs were carboxylated by adding succinic anhydride (5 mg/mL) and stirring for 4 h. The carboxyl-terminated CSNs were washed with ethanol and $H_2O$ several times and dispersed in MES buffer (0.01 M, pH = 6.0) for further use. The carboxyl-terminated CSNs were functionalized with SmAb through classical carbodiimide coupling reaction. In brief, 1 mL of $CDs/SiO_2$ spheres (1 mg/mL) in MES buffer (0.01 M, pH = 6.0) was first activated by adding EDC (4 mg) and NHS (6 mg) and reacted for 15 min. The activated particles were washed with water and redispersed in 0.5 mL of HEPES buffer (0.01 M, pH = 7.4). Then, 0.5 mL of SmAb at a concentration of 150 $\mu$g/mL was added and incubated at 25 °C for 2 h with gentle agitation. The SmAb-labeled $CDs/SiO_2$, that is, iCSNs were harvested by centrifugation, and redispersed in 1 mL of HEPES buffer (0.01 M, pH = 7.4, containing 1% BSA) to form the storage dispersion and kept at 4 °C.

**Lateral Flow Test Strip Preparation.** The lateral flow test strip consists of a sample pad (8 × 3 mm), an NC membrane (25 × 3 mm), an absorbent pad (21 × 4 mm), and a black plastic adhesive card. Sample pads were soaked in the treatment solution, which was composed of PBS (10 mM, pH = 7.4) containing 1% (v/v) Tirton X-100 and 2% NaCl, and then dried at 37 °C for 2 h. SmAb (2 mg/mL) and goat antimouse IgG antibody (2 mg/mL) were separately dispersed on the T and C lines of the NC membrane using a double-headed marker (SJ001, Shenzhen Stationery Store) with an extremely small nib (SJ002, 1.97 × 34 mm, Shenzhen Stationery Store) and drying at 37 °C for 2 h. The interval between two lines was 5 mm. The sample pad, NC membrane, and absorbent pad were assembled on the black plastic adhesive card and cut into 3 mm strips. Finally, the strips were kept in an aseptic bag of 4 °C until used.

**Detection of SFTSV Using iCSN-Based Lateral Flow Test Strip.** The sample (60 $\mu$L of SFTSV NP standard solution or serum sample) was mixed with 10 $\mu$L of iCSNs in a 0.5 mL centrifuge tube. Then, the mixture was loaded onto the sample pad of the lateral flow test strip, allowing all liquid to be absorbed and migrated along the strip. After 15 min, the results were visually observed under a 360 nm UV lamp in the dry state of the test strip and photographed using an Apple cell phone camera. The images were then digitally processed using ImageJ software to detect the intensity of the T lines in the test



DOI: 10.1021/acsomega.9b03130
ACS Omega 2019, 4, 21431−21438

strips. The NC film emits blue light under the UV lamp, and the measurement of the light intensity of the T lines subtracted the light intensity of the NC film itself.

## ■ ASSOCIATED CONTENT

### Supporting Information

The Supporting Information is available free of charge at https://pubs.acs.org/doi/10.1021/acsomega.9b03130.

Apparatus, theoretical calculation of the composition of CDs, fluorescence properties of CDs, energy-dispersive X-ray pattern and element content of CSNs; results of the conjugate prepared by the glutaraldehyde method applied to the test strip; optimization of the detection condition; and summary of the analytical performances of the detection of SFTSV with different methods (PDF)

## ■ AUTHOR INFORMATION


### Corresponding Author

*E-mail: snding@seu.edu.cn. Fax: (+86) 25-52090621.

### ORCID

Qing Zhang: 0000-0002-2026-9870

Shou-Nian Ding: 0000-0003-3086-2333

Jing-Juan Xu: 0000-0001-9579-9318


### Notes

The authors declare no competing financial interest.

## ■ ACKNOWLEDGMENTS

This work was supported by the National Natural Science Foundation of China (21535003, 21575022), the National Key Research and Development Program of China (2017YFA0700404), the Key Research & Development Plan of Jiangsu Province (BE2018617), Qing Lan Project and Key Laboratory of Optic-electric Sensing and Analytical Chemistry for Life Science, MOE, Qingdao University of Science and Technology (STAM201801).

## ■ REFERENCES


(1) Yu, X.-J.; Liang, M.-F.; Zhang, S.-Y.; Liu, Y.; Li, J.-D.; Sun, Y.-L.; Zhang, L.; Zhang, Q.-F.; Popov, V. L.; Li, C.; Qu, J.; Li, Q.; Zhang, Y.-P.; Hai, R.; Wu, W.; Wang, Q.; Zhan, F.-X.; Wang, X.-J.; Kan, B.; Wang, S.-W.; Wan, K.-L.; Jing, H.-Q.; Lu, J.-X.; Yin, W.-W.; Zhou, H.; Guan, X.-H.; Liu, J.-F.; Bi, Z.-Q.; Liu, G.-H.; Ren, J.; Wang, H.; Zhao, Z.; Song, J.-D.; He, J.-R.; Wan, T.; Zhang, J.-S.; Fu, X.-P.; Sun, L.-N.; Dong, X.-P.; Feng, Z.-J.; Yang, W.-Z.; Hong, T.; Zhang, Y.; Walker, D. H.; Wang, Y.; Li, D.-X. Fever with Thrombocytopenia Associated with a Novel Bunyavirus in China. *N. Engl. J. Med.* **2011**, *364*, 1523−1532.

(2) Zhou, H.; Sun, Y.; Wang, Y.; Liu, M.; Liu, C.; Wang, W.; Liu, X.; Li, L.; Deng, F.; Wang, H.; Guo, Y.; Lou, Z. The nucleoprotein of severe fever with thrombocytopenia syndrome virus processes a stable hexameric ring to facilitate RNA encapsidation. *Protein Cell* **2013**, *4*, 445−455.

(3) Liang, X.-L.; Liu, J.-X.; Jiao, Y.-J.; Zhu, J.; Ding, S.-N. Quantitative detection of severe fever with thrombocytopenia syndrome virus via electrochemiluminescence immunoassay. *Anal. Methods* **2019**, *11*, 4197−4203.

(4) Yu, F.; Du, Y.; Huang, X.; Ma, H.; Xu, B.; Adungo, F.; Hayasaka, D.; Buerano, C. C.; Morita, K. Application of recombinant severe fever with thrombocytopenia syndrome virus nucleocapsid protein for the detection of SFTSV-specific human IgG and IgM antibodies by indirect ELISA. *Virol. J.* **2015**, *12*, 117.

(5) Yulan, S.; Mifang, L.; Jing, Q.; Cong, J.; Quanfu, Z.; Jiandong, L.; Xiaolin, J.; Qin, W.; Jing, L.; Wen, G. Early diagnosis of novel SFTS bunyavirus infection by quantitative real-time RT-PCR assay. *J. Clin. Virol.* **2012**, *53*, 48−53.

(6) Zuo, J.-Y.; Jiao, Y.-J.; Zhu, J.; Ding, S.-N. Rapid Detection of Severe Fever with Thrombocytopenia Syndrome Virus via Colloidal Gold Immunochromatography Assay. *ACS Omega* **2018**, *3*, 15399−15406.

(7) Hu, L.-M.; Luo, K.; Xia, J.; Xu, G.-M.; Wu, C.-H.; Han, J.-J.; Zhang, G.-G.; Liu, M.; Lai, W.-H. Advantages of time-resolved fluorescent nanobeads compared with fluorescent submicrospheres, quantum dots, and colloidal gold as label in lateral flow assays for detection of ractopamine. *Biosens. Bioelectron.* **2017**, *91*, 95−103.

(8) Mei, Z.; Qu, W.; Deng, Y.; Chu, H.; Cao, J.; Xue, F.; Zheng, L.; El-Nezamic, H. S.; Wu, Y.; Chen, W. One-step signal amplified lateral flow strip biosensor for ultrasensitive and on-site detection of bisphenol A (BPA) in aqueous samples. *Biosens. Bioelectron.* **2013**, *49*, 457−461.

(9) Liu, H.; Zhan, F.; Liu, F.; Zhu, M.; Zhou, X.; Xing, D. Visual and sensitive detection of viable pathogenic bacteria by sensing of RNA markers in gold nanoparticles based paper platform. *Bioelectronics* **2014**, *62*, 38−46.

(10) Li, X.; Li, W.; Yang, Q.; Gong, X.; Guo, W.; Dong, C.; Liu, J.; Xuan, L.; Chang, J. Rapid and Quantitative Detection of Prostate Specific Antigen with a Quantum Dot Nanobeads-Based Immunochromatography Test Strip. *ACS Appl. Mater. Interfaces* **2014**, *6*, 6406−6414.

(11) Ge, C.; Yu, L.; Fang, Z.; Zeng, L. An Enhanced Strip Biosensor for Rapid and Sensitive Detection of Histone Methylation. *Anal. Chem.* **2013**, *85*, 9343−9349.

(12) Hu, J.; Zhang, Z.-L.; Wen, C.-Y.; Tang, M.; Wu, L.-L.; Liu, C.; Zhu, L.; Pang, D.-W. Sensitive and Quantitative Detection of C-Reaction Protein Based on Immunofluorescent Nanospheres Coupled with Lateral Flow Test Strip. *Anal. Chem.* **2016**, *88*, 6577−6584.

(13) Liu, C.; Jia, Q.; Yang, C.; Qiao, R.; Jing, L.; Wang, L.; Xu, C.; Gao, M. Lateral Flow Immunochromatographic Assay for Sensitive Pesticide Detection by Using $Fe_3O_4$ Nanoparticle Aggregates as Color Reagents. *Anal. Chem.* **2011**, *83*, 6778−6784.

(14) Yang, D.; Ma, J.; Zhang, Q.; Li, N.; Yang, J.; Raju, P. A.; Peng, M.; Luo, Y.; Hui, W.; Chen, C.; Cui, Y. Polyelectrolyte-Coated Gold Magnetic Nanoparticles for Immunoassay Development: Toward Point of Care Diagnostics for Syphilis Screening. *Anal. Chem.* **2013**, *85*, 6688−6695.

(15) Wang, Z.; Yao, X.; Wang, R.; Ji, Y.; Yue, T.; Sun, J.; Li, T.; Wang, J.; Zhang, D. Label-free strip sensor based on surface positively charged nitrogen-rich carbon nanoparticles for rapid detection of Salmonella enteritidis. *Biosens. Bioelectron.* **2019**, *132*, 360−367.

(16) Yao, L.; Teng, J.; Zhu, M.; Zheng, L.; Zhong, Y.; Liu, G.; Xue, F.; Chen, W. MWCNTs based high sensitive lateral flow strip biosensor for rapid determination of aqueous mercury ions. *Biosens. Bioelectron.* **2016**, *85*, 331−336.

(17) Takalkar, S.; Baryeh, K.; Liu, G. Fluorescent carbon nanoparticle-based lateral flow biosensor for ultrasensitive detection of DNA. *Biosens. Bioelectron.* **2017**, *98*, 147−154.

(18) Qu, H.; Zhang, Y.; Qu, B.; Kong, H.; Qin, G.; Liu, S.; Cheng, J.; Wang, Q.; Zhao, Y. Rapid lateral-flow immunoassay for the quantum dot-based detection of puerarin. *Biosens. Bioelectron.* **2016**, *81*, 358−362.

(19) Foubert, A.; Beloglazova, N. V.; De Saeger, S. Comparative study of colloidal gold and quantum dots as labels for multiplex screening tests for multi-mycotoxin detection. *Anal. Chim. Acta* **2017**, *955*, 48−57.

(20) Corstjens, P. L. A. M.; van Lieshout, L.; Zuiderwijk, M.; Kornelis, D.; Tanke, H. J.; Deelder, A. M.; van Dam, G. J. Up-Converting Phosphor Technology-Based Lateral Flow Assay for Detection of Schistosoma Circulating Anodic Antigen in Serum. *J. Clin. Microbiol.* **2008**, *46*, 171−176.

(21) Yan, Z.; Zhou, L.; Zhao, Y.; Wang, J.; Huang, L.; Hu, K.; Liu, H.; Wang, H.; Guo, Z.; Song, Y.; Huang, H.; Yang, R. Rapid quantitative detection of Yersinia pestis by lateral-flow immunoassay




DOI: 10.1021/acsomega.9b03130
*ACS Omega* 2019, 4, 21431−21438

and up-converting phosphor technology-based biosensor. *Sens. Actuators, B* **2006**, *119*, 656−663.
(22) Khreich, N.; Lamourette, P.; Boutal, H.; Devilliers, K.; Créminon, C.; Volland, H. Detection of Staphylococcus enterotoxin B using fluorescent immunoliposomes as label for immunochromatographic testing. *Anal. Biochem.* **2008**, *377*, 182−188.
(23) Wen, C.-Y.; Xie, H.-Y.; Zhang, Z.-L.; Wu, L.-L.; Hu, J.; Tang, M.; Wu, M.; Pang, D.-W. Fluorescent/magnetic micro/nano-spheres based on quantum dots and/or magnetic nanoparticles: preparation, properties, and their applications in cancer studies. *Nanoscale* **2016**, *8*, 12406−12429.
(24) Huang, L.; Liao, T.; Wang, J.; Ao, L.; Su, W.; Hu, J. Brilliant Pitaya-Type Silica Colloids with Central-Radial and High-Density Quantum Dots Incorporation for Ultrasensitive Fluorescence Immunoassays. *Adv. Funct. Mater.* **2018**, *28*, 1705380.
(25) Shi, D.; Cho, H. S.; Chen, Y.; Xu, H.; Gu, H.; Lian, J.; Wang, W.; Liu, G.; Huth, C.; Wang, L.; Ewing, R. C.; Budko, S.; Pauletti, G. M.; Dong, Z. Fluorescent Polystyrene-Fe3O4Composite Nanospheres for In Vivo Imaging and Hyperthermia. *Adv. Mater.* **2009**, *21*, 2170−2173.
(26) Ye, F.; Barrefelt, Å.; Asem, H.; Abedi-Valugerdi, M.; El-Serafi, I.; Saghafian, M.; Abu-Salah, K.; Alrokayan, S.; Muhammed, M.; Hassan, M. Biodegradable polymeric vesicles containing magnetic nanoparticles, quantum dots and anticancer drugs for drug delivery and imaging. *Biomaterials* **2014**, *35*, 3885−3894.
(27) Xie, H.-Y.; Zuo, C.; Liu, Y.; Zhang, Z.-L.; Pang, D.-W.; Li, X.-L.; Gong, J.-P.; Dickinson, C.; Zhou, W. Cell-Targeting Multifunctional Nanospheres with both Fluorescence and Magnetism. *Small* **2005**, *1*, 506−509.
(28) Zhao, Y.; Ma, Y.; Li, H.; Wang, L. Composite QDs@MIP Nanospheres for Specific Recognition and Direct Fluorescent Quantification of Pesticides in Aqueous Media. *Anal. Chem.* **2012**, *84*, 386−395.
(29) Li, H.; Li, Y.; Cheng, J. Molecularly Imprinted Silica Nanospheres Embedded CdSe Quantum Dots for Highly Selective and Sensitive Optosensing of Pyrethroids. *Chem. Mater.* **2010**, *22*, 2451−2457.
(30) Folarin, E.; Ken-Tye, Y.; Indrajit, R.; Rui, H.; Wing-Cheung, L.; Weiwei, Z.; Hong, D.; Fang, W.; Rajiv, K.; Swihart, M. T. In Vivo Targeted Cancer Imaging, Sentinel Lymph Node Mapping and Multi-Channel Imaging with Biocompatible Silicon Nanocrystals. *ACS Nano* **2011**, *5*, 413−423.
(31) Zheng, D.; zhang, G.; Wang, X. Integrating CdS quantum dots on hollow graphitic carbon nitride nanospheres for hydrogen evolution photocatalysis. *Appl. Catal., B* **2015**, *179*, 479−488.
(32) Tomczak, N.; Jańczewski, D.; Han, M.; Vancso, G. J. Designer polymer-quantum dot architectures. *Prog. Polym. Sci.* **2009**, *34*, 393−430.
(33) Wiriyachaiporn, N.; Sirikett, H.; Maneeprakorn, W.; Dharakul, T. Carbon nanotag based visual detection of influenza A virus by a lateral flow immunoassay. *Microchim. Acta* **2017**, *184*, 1827−1835.
(34) Huang, Y.; Wu, T.; Wang, F.; Li, K.; Qian, L.; Zhang, X.; Liu, G. Magnetized Carbon Nanotube Based Lateral Flow Immunoassay for Visual Detection of Complement Factor B. *Molecules* **2019**, *24*, 2759.
(35) Qiu, W.; Baryeh, K.; Takalkar, S.; Chen, W.; Liu, G. Carbon nanotube-based lateral flow immunoassay for ultrasensitive detection of proteins: application to the determination of IgG. *Microchim. Acta* **2019**, *186*, 436.
(36) Baker, S. N.; Baker, G. A. Luminescent Carbon Nanodots: Emergent Nanolights. *Angew. Chem., Int. Ed.* **2010**, *49*, 6726−6744.
(37) Sun, Y.-P.; Zhou, B.; Lin, Y.; Wang, W.; Fernando, K. A. S.; Pathak, P.; Meziani, M. J.; Harruff, B. A.; Wang, X.; Wang, H.; Luo, P. G.; Yang, H.; Kose, M. E.; Chen, B.; Veca, L. M.; Xie, S.-Y. Quantum-Sized Carbon Dots for Bright and Colorful Photoluminescence. *J. Am. Chem. Soc.* **2006**, *128*, 7756−7757.
(38) Yang, S.-T.; Cao, L.; Luo, P. G.; Lu, F.; Wang, X.; Wang, H.; Meziani, M. J.; Liu, Y.; Qi, G.; Sun, Y.-P. Carbon Dots for Optical Imaging in Vivo. *J. Am. Chem. Soc.* **2009**, *131*, 11308−11309.
(39) Wang, F.; Xie, Z.; Zhang, H.; Liu, C.-y.; Zhang, Y.-g. Highly Luminescent Organosilane-Functionalized Carbon Dots. *Adv. Funct. Mater.* **2011**, *21*, 1027−1031.
(40) Geng, X.; Sun, Y.; Li, Z.; Yang, R.; Zhao, Y.; Guo, Y.; Xu, J.; Li, F.; Wang, Y.; Lu, S.; Qu, L. Retrosynthesis of Tunable Fluorescent Carbon Dots for Precise Long-Term Mitochondrial Tracking. *Small* **2019**, No. e1901517.
(41) Liu, H.; Yang, J.; Li, Z.; Xiao, L.; Aryee, A. A.; Sun, Y.; Yang, R.; Meng, H.; Qu, L.; Lin, Y.; Zhang, X. Hydrogen-Bond-Induced Emission of Carbon Dots for Wash-Free Nucleus Imaging. *Anal. Chem.* **2019**, *91*, 9259−9265.
(42) Liu, H.; Sun, Y.; Li, Z.; Yang, J.; Aryee, A. A.; Qu, L.; Du, D.; Lin, Y. Lysosome-targeted carbon dots for ratiometric imaging of formaldehyde in living cells. *Nanoscale* **2019**, *11*, 8458−8463.
(43) Tang, J.; Kong, B.; Wu, H.; Xu, M.; Wang, Y.; Wang, Y.; Zhao, D.; Zheng, G. Carbon Nanodots Featuring Efficient FRET for Real-Time Monitoring of Drug Delivery and Two-Photon Imaging. *Adv. Mater.* **2013**, *25*, 6569−6574.
(44) Zhao, H. X.; Liu, L. Q.; Liu, Z. D.; Wang, Y.; Zhao, X. J.; Huang, C. Z. Highly selective detection of phosphate in very complicated matrixes with an off-on fluorescent probe of europium-adjusted carbon dots. *Chem. Commun.* **2011**, *47*, 2604−2606.
(45) Li, H.; He, X.; Kang, Z.; Huang, H.; Liu, Y.; Liu, J.; Lian, S.; Tsang, C. H. A.; Yang, X.; Lee, S.-T. Water-Soluble Fluorescent Carbon Quantum Dots and Photocatalyst Design. *Angew. Chem., Int. Ed.* **2010**, *49*, 4430−4434.
(46) Liu, Y.; Liu, C.-y.; Zhang, Z.-y.; Yang, W.-d.; Nie, S.-d. Plasmon-enhanced photoluminescence of carbon dots-silica hybrid mesoporous spheres. *J. Mater. Chem. C* **2015**, *3*, 2881−2885.
(47) Xie, Z.; Wang, F.; Liu, C.-y. Organic-Inorganic Hybrid Functional Carbon Dot Gel Glasses. *Adv. Mater.* **2012**, *24*, 1716−1721.
(48) Thomas, J. K. Physical Aspects of Radiation-Induced Processes on SiO2, γ-Al2O3, Zeolites, and Clays. *Chem. Rev.* **2005**, *105*, 1683−1734.
(49) Xu, X.; Han, Y.; Li, D.; Ding, H.; Wang, Y.; Xiao, F.-S. Improved Structural Order, Stability, and Anion-Exchange Capacity of Cation-Mediated Bridged Hybrid Mesoscopic Materials by Using Chelating Ligands. *Chem. Mater.* **2004**, *16*, 3507−3512.
(50) Chen, Y.; Zheng, M.; Xiao, Y.; Dong, H.; Zhang, H.; Zhuang, J.; Hu, H.; Lei, B.; Liu, Y. A Self-Quenching-Resistant Carbon-Dot Powder with Tunable Solid-State Fluorescence and Construction of Dual-Fluorescence Morphologies for White Light-Emission. *Adv. Mater.* **2016**, *28*, 312−318.
(51) Ding, Z.; Di, L.; Jing, P.; Zhai, Y.; Shen, D.; Qu, S.; Rogach, A. L.; Ding, Z.; Di, L.; Jing, P. Conquering Aggregation-Induced Solid-State Luminescence Quenching of Carbon Dots through a Carbon Dots-Triggered Silica Gelation Process. *Chem. Mater.* **2017**, *29*, 1779−1787.
(52) Reif, O.-W.; Nier, V.; Bahr, U.; Freitag, R. Immobilized metal affinity membrane adsorbers as stationary phases for metal interaction protein separation. *J. Chromatogr. A* **1994**, *664*, 13−25.
(53) Kubota, N.; Nakagawa, Y.; Eguchi, Y. Recovery of serum proteins using cellulosic affinity membrane modified by immobilization of $Cu^{2+}$ ion. *J. Appl. Polym. Sci.* **1996**, *62*, 1153−1160.


DOI: 10.1021/acsomega.9b03130
*ACS Omega* 2019, 4, 21431−21438